

Spectroscopic and Quantum Chemical Investigations of Hypothetical *m*-Diacetylaminoazopyrimidine and Its Photovoltaic Properties

Hitler Louis, Israel Solomon Etim, Nelson Ibe Nzeata and Ayuk Usaji Atu

Department of Pure and Applied Chemistry, Faculty of Physical Sciences, University of Calabar, Calabar, Nigeria.

Doi: <https://doi.org/10.47011/14.2.5>

Received on: 17/03/2020;

Accepted on: 09/06/2020

Abstract: Here, an attempt is made to theoretically study and predict the electronic and spectroscopic (UV-Vis and IR) and structural properties, quantum chemical descriptors and subsequent application of diacetylaminoazopyrimidine in dye-sensitized solar cells (DSSCs). Ground- and excited-state time-dependent density functional theory (TD-DFT) calculations were carried out using material studio and ORCA software, respectively. The computed ground-state energy gap, chemical hardness, chemical softness, chemical potential, electronegativity and electrophilicity index are: 3.60 eV, 1.80 eV, 0.56 eV, 4.49 eV, -4.49 eV and 5.68, respectively. Conversely, the DFT-predicted excited-state quantum chemical descriptors are: 1.67 eV, 0.83 eV, 1.20 eV, 4.71 eV and -4.71 eV, corresponding to the energy gap, chemical hardness, chemical softness, chemical potential and electronegativity, respectively. Furthermore, vibrational frequency calculations confirm the presence of some key functional groups (N=N, C=O, C-H) present in the dye molecules. The computed optoelectronic parameters, such as light-harvesting efficiency, electron injection and open-circuit voltage are 0.06 eV, -8.59 eV and -5.75 eV, respectively. Overall, the dye possesses a relatively good current conversion efficiency as compared to other dyes studied in the literature; hence, it could be used as a novel material for photovoltaic technological applications.

Keywords: Diacetylaminoazopyrimidine, DFT, Excited state, Spectroscopy, DSSCs.

1. Introduction

Azo and azo-related functional groups form a highly colored class of organic compounds which are often utilized as dyes and pigments. They have attracted much attention and have been widely used in many practical applications, such as coloring fibers [1, 2], photo-electronic applications [3], printing systems [4, 5], optical storage technology [6,7], textile dyes [8-10], as well as in many biological reactions [11-13] and in analytical chemistry [14, 16]. Dye-sensitized solar cells (DSSCs) have been considered with significance interest due to the fascinating low cost of the conversion of photovoltaic energy compared to silicon-based semiconductor solar cells, as well as the availability of the raw

materials used for the fabrication of DSSC devices [17, 18]. Among other importance aspects, DSSCs utilize wide band-gap semiconductors, sensitized (dye molecules), transparent conductive oxide layers (TCO) and electrolytes (typically iodide/triiodide) [19]. The basic operational principles involve first the trapping of solar radiation by the dye molecules in the visible region of the spectrum, followed by the electronic excitation into the conductive band of the semiconductor; finally, an electron is regenerated to the dye by the redox electrolyte [20, 21].

To the best of our knowledge, neither quantum chemical calculations nor spectroscopic

investigations have yet been performed on diacetylaminopyrimidine, which is the motivating factor to carry out this investigation. Herein, quantum chemical calculations were performed in order to investigate the electronic structural properties (energy gap, charge distribution calculations), spectroscopic (UV/Vis, IR) properties, prediction of the quantum chemical descriptors (global reactivity descriptors, some geometrical parameters, such as bond lengths and bond angles), and subsequent prediction of photovoltaic properties of m-diacetylaminopyrimidine for possible application in DSSCs. Electronic absorption spectra of m-diacetylaminopyrimidine were computed and predicted by applying the time-dependent density functional theory (TD-DFT) computational method which gives information on the calculation of electronic excitation energies, oscillator strengths, total energies and maximum wavelength of absorption.

2. Computational Details

In order to obtain stable structures, the geometrical parameters of m-diacetylaminopyrimidine dye molecule (as shown in Fig. 1) in the ground state were optimized at DFT theory level using DMol3 material studio program with the dnd basis set. The frontier orbital gap helps characterize the chemical reactivity and the kinetic stability of the molecule. A molecule with a small frontier orbital gap is generally associated with a high chemical reactivity; low kinetic stability is termed as soft molecule [22]. In these processes, the potentially interesting electronic transitions are those involving narrow energy gaps. Both the Higher Occupied Molecular Orbitals (HOMO) and the Lower Unoccupied Molecular Orbitals (LUMO) are the main orbitals that take part in chemical stability. HOMO represents the ability to donate an electron, while LUMO as an electron acceptor represents the ability to acquire an electron. This electron absorption corresponds to the transition from the ground state to the first excited state and is mainly described by one electron excitation from the HOMO to the LUMO. The energy of the HOMO is directly related to the ionization potential, while LUMO energy is directly related to the electron affinity. The HOMO-LUMO analysis has been carried out to explain the charge transfer within m-diacetylaminopyrimidine.

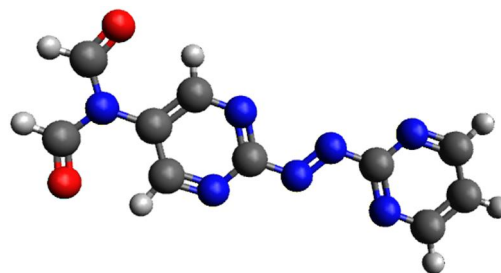


FIG. 1. Structure of m-diacetylaminopyrimidine dye molecule (the red, black, blue and white colors stand for oxygen, carbon, nitrogen and hydrogen, respectively).

HOMO and LUMO are very important parameters for quantum chemistry along with excited-state investigations. The investigation of the way the molecule interacts with other species could be elucidated from the HOMO-LUMO. HOMO, which can be thought of as the outermost orbitals containing electrons, tends to give electrons as an electron donor. On the other hand, LUMO can be thought of as the innermost orbitals containing free orbital to accept electrons. The HOMO-LUMO analysis has been carried out to explain the charge transfer within m-diacetylaminopyrimidine through the excited-state calculations with material studio.

Chemical hardness demonstrates the resistance to alteration in electron distribution. Chemical hardness formula is well correlated with the stability and reactivity of the chemical system [23]:

$$\eta = \frac{(E_{\text{LUMO}} - E_{\text{HOMO}})}{2}. \quad (1)$$

Following Parr and Pearson [24], the electronic chemical potential describes the escaping tendency of electrons from a stable system. Thus, its formula is:

$$\mu = -\frac{(E_{\text{HOMO}} + E_{\text{LUMO}})}{2}. \quad (2)$$

Chemical hardness demonstrates the resistance to alteration in electron distribution and chemical softness is an inverse of it. Chemical softness is also related with the stability and reactivity of the chemical system [23]:

$$S = \frac{1}{\eta}. \quad (3)$$

Electronegativity is described as the negative of electronic chemical potential. Since chemical potential describes the escaping tendency of

electrons from a stable system, electronegativity describes the retaining tendency of an electron in a stable system. The formula is thus [23]:

$$\chi = \frac{(E_{\text{HOMO}} + E_{\text{LUMO}})}{2}. \quad (4)$$

The global electrophilicity index introduced by Parr [23] is calculated in terms of chemical potential and hardness. It assesses the lowering of energy due to maximal electron flow between donor and acceptor. The formula is thus:

$$\omega = \mu^2 / 2\eta. \quad (5)$$

3. Results and Discussion

3.1. Geometrical Parameters

The optimized geometry of m-diacetylaminopyrimidine was obtained using material studio program and DFT method in gas phase. The structural properties (of the optimized geometrical parameters) which include bond distance and bond angle of the m-diacetylaminopyrimidine molecule in gas phase were obtained and reported in Tables 1 and 2. The total description of the molecular geometry of m-diacetylaminopyrimidine molecule in gas phase was obtained using *ab initio* and DFT method. From the optimized results, it is shown that there is no distortion in the structure and the angles are perfectly hexagonal for the heterocyclic compound (pyrimidine) molecule. This is due to the fact that there was no excitation in the ground state; therefore, the aromatic ring of pyrimidine is remaining unchanged. Also, the diacetyl amino group bonded to azopyrimidine did not act as a withdrawing group in ground state. The bond angles and distances were retained at the ground-state optimization, as shown in Tables 1 and 2. Table 1 shows that nonbonding distances from H2 to H1 and from H3 to H4 with values 2.561 Å and 2.520 Å are the highest bond distances. The least bond distance is 1.085 Å between C8-N6 atoms. From Table 2, the largest bond angle is 126.276° between the atoms of N2-C1-N1, while the least bond angle is 110.492° between the atoms of N3-C5-H3. The values obtained from the optimization are equivalent to the values obtained by Ali and coworkers [25].

TABLE 1. Ground-state bond distances in gas phase.

Bond distance	Gas phase reading in ground state (Å)
A1 (O1=C6)	1.196
A2 (C6-H2)	1.103
A3 (H2 H1)	2.561
A4 (C6-N3)	1.420
A5 (N3-C3)	1.421
A6 (N3-C5)	1.419
A7 (C5=O2)	1.196
A8 (C5-H3)	1.103
A9 (H3 H4)	2.520
A10 (C3=C2)	1.392
A11 (C2-H1)	1.086
A12 (C2-N1)	1.325
A13 (N1=C1)	1.334
A14 (C1-N2)	1.332
A15 (N2=C4)	1.323
A16 (C4-H4)	1.086
A17 (C1-N4)	1.428
A18 (N4=N5)	1.241
A19 (N5-C7)	1.430
A20 (C7=N7)	1.330
A21 (N7-C10)	1.330
A22 (C10-H5)	1.085
A23 (C10=C9)	1.387
A24 (C9-H6)	1.081
A25 (C9-C8)	1.387
A26 (C8-H7)	1.085
A27 (C8=N6)	1.332
A28 (N6-C7)	1.330

TABLE 2. Ground-state bond angles in gas phase.

Bond angle/degrees	Gas phase reading in ground state/degrees
B1 (O1=C6-H2)	123.872
B2 (O1=C6-N3)	125.618
B3 (H2-C6-N3)	110.510
B4 (C6-N3-C5)	123.009
B5 (C6-N3-C3)	118.362
B6 (N3-C3=C2)	121.695
B7 (N3-C3-C4)	122.185
B8 (N3-C5=O2)	125.952
B9 (N3-C5-H3)	110.492
B10 (O2=C5-H3)	123.555
B11 (H1-C2=C3)	120.548
B12 (H1-C2-N1)	117.343
B13 (C2=C3-C4)	116.111
B14 (C2-N1=C1)	116.621
B15 (C3=C2-N1)	122.108
B16 (C3-C4-H4)	120.596
B17 (C3-C4=N2)	122.328
B18 (H4-C4=N2)	117.074
B19 (C4=N2-C1)	116.459
B20 (N2-C1=N1)	126.276

Bond angle/degrees	Gas phase reading in ground state/degrees
B21 (N2-C1-N4)	120.724
B22 (N1=C1-N4)	112.874
B23 (C1-N4=N5)	114.344
B24 (N4=N5-C7)	112.448
B25 (N5-C7=N7)	118.177
B26 (N5-C7-N6)	113.978
B27 (C7-N6-C8)	115.596
B28 (C7=N7-C10)	115.407
B29 (N7-C10-H5)	116.379
B30 (N7-C10=C9)	122.433
B31 (H5-C10=C9)	121.185
B32 (C10=C9-H6)	121.572
B33 (C10=C9-C8)	116.577
B34 (H6-C9-C8)	121.847
B35 (C9-C8-H7)	121.307
B36 (C9-C8=N6)	122.149
B37 (H7-C8=N6)	116.541

3.2 Analysis of Frontier Molecular Orbitals

According to the interaction between the highest occupied molecular orbitals (HOMO) and the lowest unoccupied molecular orbitals (LUMO) of a structure, transitions of type $\pi - \pi^*$ are observed according to the molecular orbital theory. The calculated energy value for m-diacetylaminopyrimidine in ground state, gas phase are; $E_{\text{HOMO}} = -6.298$ eV, $E_{\text{LUMO}} = -2.697$ eV, $\Delta E = 3.601$ eV. The calculated energy value for m-diacetylaminopyrimidine in excited state, gas phase are; $E_{\text{HOMO}} = -5.540$ eV, $E_{\text{LUMO}} = -3.875$ eV, $\Delta E = 1.665$ eV. As can be seen from the calculated results of m-diacetylaminopyrimidine molecule at ground state and excited state, the energy gap is less than 4 as compared with the energy gap obtained by Yossa [26] which is greater than 4; therefore showing that our molecule is soft, can be reactive in many electronic devices and has a lower chemical reactivity with high kinetic stability. According to Demircioglu *et al.* [27], the narrow energy gap between HOMO and LUMO facilitates of the dye molecule makes the material nonlinear and optically active.

3.3 Chemical Descriptors

Comparing chemical hardness and softness, it would be observed that chemical hardness demonstrates the resistance to alteration in electron distribution in a chemical system, while chemical softness is related with the stability and reactivity of the chemical system. Chemical hardness obtained from the calculation was 1.8005 eV, whereas the calculated chemical

softness related with the stability and reactivity of the chemical system was 0.5554 eV. These obtained results show that the chemical hardness of m-diacetylaminopyrimidine at the ground state is greater than chemical softness. At the excited state, chemical hardness obtained from the calculation was 0.8325 eV, while the calculated chemical softness related with the stability and reactivity of the chemical system was 1.2012 eV. From the obtained values also, it is shown that chemical hardness is greater than chemical softness at the ground state, while chemical softness is greater than chemical hardness at the excited state. Therefore, m-diacetylaminopyrimidine at the ground state will demonstrate resistance to alteration in electron distribution in a chemical system, while at the excited state, it will demonstrate stability and reactivity when compared with Demircioglu's work [27].

Following Parr *et al.* [23], the electronic chemical potential describes the escaping tendency of electrons from a stable system and electronegativity describes the retaining tendency of an electron in a stable system. The chemical potential obtained from the calculated results of HOMO and LUMO at ground state was 4.498 eV and that obtained from the calculated value of electronegativity which is the negative value of electronic chemical potential was -4.498 eV. Also, the chemical potential obtained from the calculated results of HOMO and LUMO in the excited state was 4.7075 eV. In addition, the calculated value of electronegativity, which represents the negative value of electronic chemical potential, was found to be -4.7075 eV. The opposite values for both ground and excited states show that the electrons from a stable system will maintain their energy level without escaping [27]. According to Yossa *et al.* [26], a high value of chemical potential and electrophilicity characterizes a good electrophile, whereas a small value stands for a good nucleophile.

The global electrophilicity index assesses the lowering of energy due to maximal electron flow between donor and acceptor. The value obtained from the calculation as from chemical hardness and potential at ground-state level was 5.6184 eV. From the values of chemical potential of 4.498 eV, chemical hardness of 1.8005 eV and electrophilicity of 5.618 eV at ground-state level, electrophilicity aids in obtaining the energy of

assessing through chemical potential and hardness of the electrons. Also, the value obtained at the excited state for global electrophilicity index was 13.3096 eV. From the values of chemical potential of 4.7075 eV, chemical hardness of 0.8325 eV and electrophilicity of 13.3096 eV in the excited state level, we will have excess energy of assessing through chemical potential and hardness of the electrons. According to Yossa *et al.* [26], it is shown that m-diacetylaminoazopyrimidine is a good electrophile at the excited state and a good nucleophile at the ground state.

3.4 Mulliken Population Analyses

The calculation of atomic charges plays an important role in the application of quantum mechanical calculations to molecular systems [28]. Our interest here is in the comparison of different states of Mulliken charges to describe the electron distribution in m-diacetylaminoazopyrimidine compound as broadly as possible and assess the sensitivity of the calculated charges to changes in the choice

of the basis set. Mulliken charges are calculated by determining the electron population of each atom as defined in the basis functions. The intention is also to accurately model partial charge magnitude and location within m-diacetylaminoazopyrimidine. Mulliken analysis is a good way to account for differences in electronegativities of atoms within the molecule and use it to support Fukui analysis. The charge calculations are reported in Table 3. These results show that the Mulliken charges at complete convergence are greater and longer than the Mulliken charges at convergence. Therefore, the distribution of charges at Mulliken complete convergence will be much more rapid than the charges at Mulliken convergence. The choice of dnd basis set of material studio program is reliable, as it distinguishes clearly between the two convergences of Mulliken charges. From the population analysis, it was generally observed that 14 atoms are positively charged while 12 atoms are negativity charged.

TABLE 3. Mulliken atomic charges reading

Atom	Mulliken charges at convergence	Mulliken charges at complete convergence
C8	-0.041	-0.039
C9	0.283	0.286
C3	-0.044	-0.043
N7	-0.319	-0.316
C7	0.499	0.500
N6	-0.317	-0.316
N5	-0.171	-0.152
N4	-0.172	-0.154
C1	0.511	0.512
N2	-0.344	-0.339
N1	-0.342	-0.399
C2	0.025	0.026
C3	-0.176	-0.172
C4	0.025	0.027
N3	-0.470	-0.470
C5	0.326	0.326
C6	0.328	0.328
O1	-0.356	-0.352
O2	-0.355	-0.351
H3	0.138	0.139
H2	0.139	0.140
H4	0.174	0.179
H1	0.174	0.178
H7	0.162	0.167
H5	0.162	0.168
H6	0.161	0.168

3.5 Fukui Results and Analysis

The local reactivity descriptor like Fukui function indicates the preferred regions where a chemical species (molecule) will amend its density when the numbers of electrons are modified; or it indicates the tendency of the electronic density to deform at a given position upon accepting or donating electrons [23]. The condensed or atomic Fukui functions on the j_{th} atom site, for electrophilic $f_j^-(r)$, nucleophilic $f_j^+(r)$ and free radical f_j^0 attacks are defined as $f_j^0 f_j^+ = q_j(N + 1) - q_j, f_j^- = q_j(N) - q_j(N - 1)$ and $f_j^0 = 0.5[q_j(N + 1) - q_j(N - 1)]$ respectively, where q_j is the atomic charge (Mulliken or Hirshfeld) at the j_{th} atomic site in the anionic ($N + 1$), cationic ($N - 1$) or neutral molecule. Parr *et al.* [23] showed that sites in chemical species with the largest values of Fukui function (f_j) show high reactivity for corresponding attacks. The Fukui functions calculated from the Mulliken and Hirshfeld charges have been reported to be in good agreement [29]. The values of calculated Fukui functions for the electrophilic, nucleophilic and radical attack, as reported in Tables 4, 5 and 6,

respectively, indicate that in *m*-diacetylaminoazopyrimidine, the reactivity order for the nucleophilic case is $N4 > N5 > C9 > H5 > H1 > H4 > H7 > C3 > N6 > H6 > O1 > O2 > N7 > N2 > C7 > N1 > N7 > C8 > C2 > C4 > H3 > H2 > C6 > C5 > C1$ and the electrophilic reactivity order is $N5 > N4 > H5 > H6 > H7 > N2 > O2 > O1 > H4 > H1 > C3 > C9 > N1 > N7 > C8 > C4 > C2 > C3 > H3 > H2 > N6 > C6 > C5 > C7 > C1 > N3$, while the order of sites for free radical attack is $N4 > N5 > H5 > C9 > H7 > H6 > H1 > H4 > O2 > O1 > C3 > N2 > N7 > N6 > N1 > C3 > C7 > C8 > C2 > C4 > H3 > H2 > C5 > C6 > C1$. The local softness condensed to an atom location is defined by $s_j^\pm = f_j^\pm$ [30] and local electrophilicity indices are defined by $w_j^\pm = f_j^\pm w$ [31] and are also calculated to illustrate the reactivity of atoms. These equations envisage the most electrophilic site in a system having the maximum value of s^+ and w^+ , while maximum value of s^- and w^- corresponds to the nucleophilic site in the molecule. The local reactivity descriptors, like s_j^\pm and w_j^\pm , provide the reactivity tendencies of local site during nucleophilic or electrophilic attacks.

TABLE 4. Fukui electrophilic attack (f_j^-).

Atom	Mulliken	Hirshfeld
C8	0.018	0.029
C9	0.035	0.039
C3	0.016	0.028
N7	0.026	0.029
C7	0.005	0.008
N6	0.010	0.020
N5	0.186	0.182
N4	0.178	0.176
C1	0.004	0.016
N2	0.048	0.047
N1	0.028	0.033
C2	0.017	0.038
C3	0.039	0.058
C4	0.018	0.038
N3	0.001	0.007
C5	0.005	0.009
C6	0.005	0.010
O1	0.044	0.041
O2	0.044	0.041
H3	0.011	0.007
H2	0.010	0.007
H4	0.043	0.023
H1	0.042	0.022
H7	0.053	0.029
H5	0.058	0.033
H6	0.055	0.030

TABLE 5. Fukui nucleophilic attack (f_j^+).

Atom	Mulliken	Hirshfeld
C8	0.018	0.035
C9	0.066	0.062
C3	0.027	0.042
N7	0.041	0.046
C7	0.031	0.041
N6	0.047	0.048
N5	0.123	0.119
N4	0.142	0.136
C1	0.003	0.017
N2	0.034	0.036
N1	0.028	0.031
C2	0.014	0.035
C3	0.047	0.059
C4	0.012	0.032
N3	-0.005	0.005
C5	0.006	0.011
C6	0.006	0.010
O1	0.046	0.043
O2	0.045	0.042
H3	0.010	0.007
H2	0.009	0.006
H4	0.050	0.026
H1	0.052	0.028
H7	0.048	0.026
H5	0.054	0.032
H6	0.046	0.025

TABLE 6. Fukui free radical attack (f_j^0).

Atom	Mulliken	Hirshfeld
C8	0.018	0.032
C9	0.051	0.051
C3	0.022	0.035
N7	0.034	0.037
C7	0.018	0.024
N6	0.029	0.034
N5	0.154	0.151
N4	0.160	0.156
C1	0.004	0.017
N2	0.041	0.042
N1	0.028	0.032
C2	0.016	0.037
C3	0.043	0.059
C4	0.015	0.035
N3	-0.002	0.006
C5	0.006	0.010
C6	0.005	0.010
O1	0.045	0.042
O2	0.045	0.042
H3	0.011	0.007
H2	0.010	0.006
H4	0.047	0.025
H1	0.047	0.025
H7	0.050	0.027
H5	0.056	0.032
H6	0.050	0.028

From Table 4, Fukui electrophilic attacks at C8 down to C6 are greater at Hirshfeld charges than at Mulliken charges and Fukui electrophilic attacks at O1 to H6 are greater at Mulliken charges than at Hirshfeld charges. This shows that as Fukui electrophilic attack descends according to converging, the Mulliken charges become greater than the Hirshfeld charges. But at N5 and N4, Fukui electrophilic attacks for Mulliken charges are greater than for Hirshfeld charges for C8 to C6 range. According to Parr *et al.* [23], N5 for Mulliken is the indicated region for Fukui electrophilic attack, while N5 for Hirshfeld is also the indicated region for Fukui electrophilic attack.

A quick look at the results presented in Table 5 shows that Fukui nucleophilic attack at C9 is weak for Hirshfeld charges and strong for Mulliken charges. At N3, Fukui nucleophilic attack is weak for Mulliken charges and strong for Hirshfeld charges. From C8 down to C6 except C9, Fukui nucleophilic attack for Hirshfeld charges is greater than for Mulliken charges. And from O1 to H6, Fukui nucleophilic attacks for Mulliken charges are greater than for Hirshfeld charges. But Fukui nucleophilic attack for Mulliken charges at N5 and N4 is greater than for Hirshfeld charges. According to Parr *et al.* [23], N4 for Mulliken is the indicated region for Fukui nucleophilic attack, while N4 for Hirshfeld is also the indicated region for Fukui nucleophilic attack.

As reported in Table 6, the Fukui free radical attack is greater for Hirshfeld charges than for Mulliken charges from C8 down to C6. And Fukui free radical attacks at O1 to H6 for Mulliken charges are greater than for Hirshfeld charges. But Fukui free radical attacks at N5 and N4 for Mulliken charges are greater than for Hirshfeld charges. According to Parr *et al.* [23], N4 for Mulliken is the indicated region for Fukui radical attack, while N4 for Hirshfeld is also the indicated region for Fukui radical attack.

3.6 Electrostatic Potential (ESP) Fitted Charges

According to Muller [32], although Mulliken charges are adequate for approximating the charge on an atom, the charges generated are very basis set-dependent. A far better approach is electrostatic potential (ESP) fitting, which calculates the electrostatic potential at each point on a grid outside the molecule and then fits a set

of charges at the atoms to reproduce that potential.

As reported in Table 7, it is shown that C7 carries the highest charge followed by C1 > C3 > C8 > C2 > C4 > C6 > C5 > H5 > N3 > H6 > H7 > H3 = H2 > H4 > H1. This shows that the most positively charged atom is C7 and the most negatively charged atom is O1 m-diacetylaminoazopyrimidine.

TABLE 7. ESP fitted charges.

Atoms	ESP-fitted charges
C8	0.583
C9	-0.732
C3	0.619
N7	-0.890
C7	1.429
N6	-0.837
N5	-0.430
N4	-0.387
C1	1.296
N2	-0.806
N1	-0.755
C2	0.494
C3	-0.645
C4	0.446
N3	0.113
C5	0.329
C6	0.333
O1	-0.383
O2	-0.386
H3	0.061
H2	0.061
H4	0.057
H1	0.050
H7	0.069
H5	0.232
H6	0.079

3.7 Time-dependent Density Functional Theory (TD-DFT)

Time-dependent Density Functional Theory (TD-DFT) is a quantum mechanical theory used in physics and chemistry to investigate the properties and dynamics of many-body systems in the presence of time-dependent potentials. From the definition, the TD-DFT tabulated result (reported in Tables 8 and 9) shows an abrupt increase in eigenvalues (that is, for au and eV) from state 4 to state 5 with different spin (+ to -) orientation; same increase in eigenvalues occurs from state 18 to state 19 with same spin (- to -) orientation, then comes a drastic increment from state 38 to state 39 with the same spin (- to -) orientation. The dynamics studies show that an increase in eigenvalues can occur within a

system as a result of change in atom absorption and excitation. The positively charged eigenvalues are those of state 147 to state 148 with spin (+ to -) orientation; therefore, they are of the highest energy.

The TD-DFT excitation result in Table 9 shows an increase in energy (eV) down the table and a decrease in wavelength down the table. The oscillations show special features, as at the first spin level for each excitation a zero oscillation is observed before the second spin. Therefore, it is shown that at the first spin level, there is no oscillation and oscillations occur at the second spin level of each excitation.

TABLE 8. TD-DFT with spin unrestricted calculation.

States		Eigenvalues		
Spin		au	eV	
1	-	1	-18.761363	-510.523
2	+	1	-18.761363	-510.523
3	-	2	-18.761287	-510.521
4	+	2	-18.761287	-510.521
5	-	3	-14.064774	-382.722
6	+	3	-14.064774	-382.722
7	+	4	-14.040890	-382.072
8	-	4	-14.040890	-382.072
9	-	5	-14.040588	-382.064
10	+	5	-14.040588	-382.064
11	-	6	-14.011219	-381.265
12	+	6	-14.011218	-381.265
13	-	7	-14.010884	-381.256
14	+	7	-14.010883	-381.256
15	+	8	-13.995844	-380.846
16	-	8	-13.995843	-380.846
17	+	9	-13.995040	-380.825
18	-	9	-13.995039	-380.825
19	-	10	-10.010049	-272.387
20	+	10	-10.010049	-272.387
21	-	11	-10.010023	-272.387
22	+	11	-10.010023	-272.387
23	+	12	-9.989379	-271.825
24	-	12	-9.989378	-271.825
25	-	13	-9.977261	-271.495
26	+	13	-9.977261	-271.495
27	-	14	-9.968635	-271.260
28	+	14	-9.968635	-271.260
29	+	15	-9.962048	-271.081
30	-	15	-9.962046	-271.081
31	+	16	-9.960467	-271.038
32	-	16	-9.960467	-271.038
33	-	17	-9.942523	-270.550
34	+	17	-9.942523	-270.550
35	-	18	-9.942400	-270.547
36	+	18	-9.942400	-270.547
37	+	19	-9.912173	-269.724

States			Eigenvalues	
Spin			au	eV
38	-	19	-9.912173	-269.724
39	-	20	-1.005929	-27.373
40	+	20	-1.005929	-27.373
41	-	21	-0.991501	-26.980
42	+	21	-0.991501	-26.980
43	-	22	-0.981861	-26.718
44	+	22	-0.981861	-26.718
45	+	23	-0.9444376	-25.698
46	-	24	-0.9444376	-25.698
47	+	25	-0.919201	-25.013
48	-	26	-0.919201	-25.013
49	-	27	-0.904054	-24.601
50	+	28	-0.904054	-24.601
51	-	28	-0.849202	-23.108
52	+	29	-0.849202	-23.108
53	+	29	-0.832600	-22.656
54	-	30	-0.832600	-22.656
55	+	31	-0.770760	-20.070
56	-	31	-0.770760	-20.070
57	+	32	-0.737551	-20.973
58	-	33	-0.737551	-20.973
59	+	33	-0.685987	-18.667
60	-	34	-0.685987	-18.667
61	+	34	-0.668289	-18.185
62	-	35	-0.668289	-18.185
63	+	35	-0.631215	-17.176
64	-	36	-0.631214	-17.176
65	+	36	-0.623338	-16.962
66	-	37	-0.623338	-16.962
67	-	37	-0.614140	-16.712
68	+	38	-0.614140	-16.712
69	+	38	-0.570230	-15.517
70	-	39	-0.570230	-15.517
71	+	39	-0.538467	-14.652
72	-	40	-0.538467	-14.652
73	-	40	-0.526409	-14.324
74	+	41	-0.526408	-14.324
75	+	41	-0.521491	-14.190
76	-	42	-0.521491	-14.190
77	+	42	-0.505805	-13.764
78	-	43	-0.505804	-13.764
79	-	43	-0.487524	-13.266
80	+	44	-0.487524	-13.266
81	+	44	-0.461962	-12.571
82	-	45	-0.461961	-12.571
83	-	45	-0.456637	-12.426
84	+	46	-0.456637	-12.426
85	-	47	-0.442610	-12.044
86	+	47	-0.442610	-12.044
87	+	48	-0.427484	-11.632
88	-	48	-0.427484	-11.632
89	+	49	-0.425746	-11.585
90	-	49	-0.425746	-11.585
91	-	50	-0.416911	-11.345
92	+	50	-0.416911	-11.345

States			Eigenvalues		States			Eigenvalues	
Spin			au	eV	Spin			au	eV
93	+	51	-0.407886	-11.099	122	+	65	-0.268494	-7.306
94	-	51	-0.407886	-11.099	123	+	66	-0.260491	-7.088
95	+	52	-0.405175	-11.025	124	-	66	-0.260491	-7.088
96	-	52	-0.405175	-11.025	125	-	67	-0.233487	-6.354
97	-	53	-0.399591	-10.873	126	+	67	-0.233487	-6.354
98	+	53	-0.399591	-10.873	127	-	68	-0.226479	-6.163
99	-	54	-0.397365	-10.813	128	+	68	-0.226479	-6.163
100	+	54	-0.397365	-10.813	129	+	69	-0.221816	-6.036
101	-	55	-0.388507	-10.572	130	-	69	-0.221816	-6.036
102	+	55	-0.388507	-10.572	131	-	70	-0.203606	-5.540
103	+	56	-0.368445	-10.026	132	+	70	-0.203606	-5.540
104	-	56	-0.368445	-10.026	133	+	71	-0.142392	-3.875
105	+	57	-0.367048	-9.988	134	-	71	-0.142392	-3.875
106	-	57	-0.367048	-9.988	135	+	72	-0.105575	-2.873
107	-	58	-0.365940	-9.958	136	-	72	-0.105575	-2.873
108	+	58	-0.365940	-9.958	137	+	73	-0.091904	-2.501
109	+	59	-0.321793	-8.756	138	-	73	-0.091904	-2.501
110	-	59	-0.321793	-8.756	139	-	74	-0.085458	-2.325
111	-	60	-0.310440	-8.448	140	+	74	-0.085458	-2.325
112	+	60	-0.310440	-8.447	141	-	75	-0.069739	-1.898
113	+	61	-0.303417	-8.256	142	+	75	-0.069739	-1.898
114	-	61	-0.303416	-8.256	143	+	76	-0.040319	-1.097
115	-	62	-0.299552	-8.151	144	-	76	-0.040319	-1.097
116	+	62	-0.299552	-8.151	145	-	77	-0.016225	-0.442
117	+	63	-0.279786	-7.613	146	+	77	-0.016225	-0.442
118	-	63	-0.279786	-7.613	147	+	78	0.059585	1.621
119	+	64	-0.275061	-7.485	148	-	78	0.059585	1.621
120	-	64	-0.275061	-7.485					
121	-	65	-0.268494	-7.306					

TABLE 9. TD-DFT excitation result.

State			Eigenvalues		Oscillations (f)
From	To	Spin	TD-ex (eV)	TD-ex (nm)	
66	67	+	1.42	873	0.000000
66	67	-	1.95	634	0.027273
65	67	-	2.12	586	0.000000
65	67	+	2.21	560	0.000084
64	67	+	2.26	549	0.000000
64	67	-	2.32	535	0.001359
63	67	+	2.44	509	0.000000
63	67	-	2.56	485	0.020763
66	68	+	2.66	467	0.000000
66	68	-	2.69	461	0.001041
66	69	+	3.04	408	0.000000
66	69	+	3.05	407	0.001372

3.8 Vibrational Frequencies (IR)

The optimized structural parameters were used to compute the vibrational frequencies of m-diacetylaminoozopyrimidine at the DFT level of calculation. The proposed vibrational mode assignments are collected in Table 10. The simulated IR spectra have been plotted using pure Lorentzian band shapes with band width of

Full Width and Half Maximum of 10 cm^{-1} . All the vibrations are active in IR. The total energy distribution (TED) for each normal mode among the symmetry coordinates of the molecule was calculated. A complete assignment of the fundamentals was proposed based on the calculated TED values, infrared intensities. Reduction in the computed harmonic vibrations, though basis set-sensitive, are only marginal as

observed in the DFT values. Anyway, notwithstanding the level of calculations, it is customary to scale down the calculated harmonic frequencies in order to improve the agreement with the experiment. Due to some systematic errors, however, some sort of empirical correction of the force field is required to obtain an acceptable agreement (in the order 15–20 cm^{-1}) of calculated frequencies. In simpler molecules, global scaling (or uniform scaling) of the theoretical force field with one common scale factor may prove satisfactory [33]. It has been shown that application of multiple scale factors; that is, selective scaling of the *ab initio* calculated force field developed leads to better results and the natural coordinates constructed were defined as proposed by Pulay [34]. Following the SQMFF (Scaled Quantum Mechanical Force Field) procedure, the harmonic force field was scaled using the recommended scaling factors of Rauhut and Pulay.

C-H Vibrations

The hetero-aromatic structure shows the presence of C-H stretching vibrations in the region 3100–3000 cm^{-1} , which is the characteristic region for the ready identification of C-H stretching vibrations [35]. In this region, the bands are not affected appreciably by the nature of substituent. From the theoretical FT-IR spectrum, the band at 3074 cm^{-1} is assigned to the C-H stretching vibrations.

C=O Vibrations

C=O double bond gives rise to a very intense absorption band in IR spectrum. The position and intensity of this band range from 1870 cm^{-1} to 1540 cm^{-1} , depending on the physical state, electronic and mass effects of neighboring substituent, intra- and intermolecular interactions and conjugations [36]. In this study, the vibrational mode of C=O was found at 1835 cm^{-1} and 1590.77 cm^{-1} in gas phase.

C-N Vibrations

The vibrational wave number of C-N group as amines in IR spectrum ranges from 1350 – 1000 cm^{-1} , depending on the physical state, electronic and mass effects of neighboring substituent. In this study, the vibrational mode of C-N was found at 1158.66 cm^{-1} in gas phase.

N=N Vibrations

The vibrational wave number of N=N group in IR spectrum ranges from 1470 – 1400 cm^{-1} , depending on the physical state, electronic and mass effects of neighboring substituent. N=N vibration in this study was observed at 1431.62 cm^{-1} in gas phase.

Ring Vibrations

The ring stretching vibrations are expected within the region 1620 – 1390 cm^{-1} [37]. Most of the ring modes are altered by the substitution to aromatic ring. The band due to the C=C stretching vibrations is normally observed in the region 1625 – 1575 cm^{-1} [38-39]. In the present case, C=C vibrations were observed at 1766.66 cm^{-1} in gas phase.

TABLE 10. Infrared frequencies and vibrational assignment.

Mode	Frequency in cm^{-1}	Vibrational assignment
9	35.66	t_m C-C
10	54.35	
11	58.00	
12	89.26	
13	135.64	
14	152.07	torsion N-C-N
15	162.58	torsion N-C-N
16	213.82	torsion N-C-N
17	246.26	β C-C
18	257.78	β C-C
19	294.31	β C-C
20	307.88	β C-C
21	388.21	gamma C-C
22	388.28	gamma C-C
23	436.01	torsion C-C
24	443.07	torsion C-C

Mode	Frequency in cm ⁻¹	Vibrational assignment
25	498.20	gamma C-C
26	516.06	torsion C-C
27	565.68	torsion C-C
28	598.44	torsion C-C
29	622.53	torsion C-H
30	666.18	torsion C-H
31	688.51	torsion C-H
32	743.73	torsion C-H
33	772.19	torsion C-H
34	788.16	torsion C-H
35	811.21	torsion C-H
36	841.13	torsion C-H
37	864.52	torsion C-H
38	866.95	torsion C-H
39	935.74	torsion C-H
40	956.31	torsion C-H
41	962.62	torsion C-H
42	969.41	torsion C-H
43	976.77	torsion C-H
44	977.35	torsion C-H
45	980.02	torsion C-H
46	1003.21	β ring, C-N
47	1032.37	s C-H, C-N
48	1061.69	t C-H, C-N
49	1077.84	β C-H, C-N
50	1101.06	C-N
51	1158.66	C-N
52	1219.06	s C-N
53	1249.83	s C-N
54	1260.50	v C-N
55	1290.10	v C-N
56	1300.96	m C-N
57	1308.25	C-N
58	1354.36	v C-H
59	1374.78	w C-H
60	1387.79	r C-H
61	1406.23	N=N
62	1417.51	N=N
63	1431.62	N=N
64	1525.07	s C-H
65	1554.25	C=O
66	1558.59	C=O
67	1571.91	C=O
68	1590.77	C=O
69	1766.60	s C=O
70	1835.24	s C=O
71	2906.58	symmetry C-H
72	2982.38	symmetry C-H
73	3066.68	symmetry C-H
74	3073.07	Asymmetry C-H
75	3074.60	Asymmetry C-H
76	3130.82	Asymmetry C-H
77	3157.71	Asymmetry C-H

v - stretching, β - in-plane bending, p - scissoring, w - wagging, r - rocking, t - twisting.

3.9 Photovoltaic Properties

3.9.1 Theoretical Background

According to Honsberg *et al.* [40], the efficiency is the most commonly used parameter to compare the performance of one solar cell to that of another. Efficiency is defined as the ratio of energy output from the solar cell to input energy from the sun. In addition to reflecting the performance of the solar cell itself, efficiency depends on the spectrum and intensity of the incident sunlight and the temperature of the solar cell. Therefore, conditions under which efficiency is measured must be carefully controlled in order to compare the performance of one device to that of another. Terrestrial solar cells are measured under AM 1.5 conditions and at a temperature of 25°C. Solar cells intended for space use are measured under AM 0 conditions. Energy conversion efficiency (η) is the ratio between the useful output of an energy conversion machine and the input in energy terms. The input, as well as the useful output maybe chemical, electric power, mechanical work, light (radiation) or heat and is given as:

$$\eta = \frac{V_{OC} J_{SC} FF}{P_{in}} \quad (6)$$

where η is the efficiency, V_{OC} is the open-circuit voltage, J_{SC} is the short-circuit current and FF is the fill factor. To analyze the relationship between V_{oc} and E_{LUMO} of the dyes based on electron injection (in DSSCs) from LUMO to the conduction band of semiconductor TiO_2 (E_{CB}), the energy relationship can be expressed as follows [41]:

$$V_{OC} = E_{LUMO} - E_{CB} \quad (7)$$

From the studied dye molecule, the LUMO values of the dye molecule and the experimental conduction band value of the TiO_2 (-4.0 eV) were applied to evaluate Eq. (7). These values are sufficient for a possible efficient electron injection. The short-circuit current density (J_{sc}) in DSSCs is determined by the following equation [42]:

$$J_{SC} = LHE(\lambda) \Phi_{inject} \eta_{collect} d\lambda \quad (8)$$

where $LHE(\lambda)$ is the light-harvesting efficiency at a given wavelength, Φ_{inject} is the electron injection efficiency and $\eta_{collect}$ denotes the charge collection efficiency. In the system where there are only differences in dye, $\eta_{collect}$ can be

assumed to be constant. The LHE can be calculated through the following equation [20]:

$$LHE = 1 - 10^{-f} \quad (9)$$

where f is the oscillator strength of adsorbed dye molecules. Φ_{inject} is related to the driving force (ΔG_{inject}) of electrons injected from the excited states of dye molecules to the semiconductor (conduction band). It can be estimated as follows [43]:

$$\Delta G_{inject} = E_{OX}^{dye*} - E_{CB}^{TiO_2} = E_{OX}^{dye} + E_{O-O}^{dye} - E_{CB}^{TiO_2} \quad (10)$$

In the above equation, E_{OX}^{dye*} is the oxidation potential of the excited state, E_{OX}^{dye} is the oxidation potential of the ground state of the dye, E_{O-O}^{dye} is the vertical transition energy and $E_{CB}^{TiO_2}$ is the conduction band edge of the TiO_2 semiconductor. So, J_{sc} can be well estimated through LHE and ΔG_{inject} .

Two models can be used for the evaluation of E_{OX}^{dye*} [44]. The first implies that the electron injection occurs from the unrelaxed excited state. For this reaction path, the excited state oxidation potential can be extracted from the redox potential of the ground state, E_{OX}^{dye} , which was calculated at the dnd basis set approach and the vertical transition energy corresponding to the photo-induced intermolecular charge transfer (ICT):

$$E_{OX}^{dye*} = E_{OX}^{dye} - \lambda_{max}^{ICT} \quad (11)$$

Here, λ_{max}^{ICT} is the energy of the ICT. Note that this relation is only valid if the entropy change during the light absorption process can be neglected as reported in previous literature [45]. For the second model, one assumes that electron injection occurs after relaxation. Given this condition, E_{OX}^{dye} is expressed as follows [45]:

$$E_{OX}^{dye*} = E_{OX}^{dye} - E_{O-O}^{dye} \quad (12)$$

3.9.2 Electron Injection

The description of the electron transfer from a dye to a semiconductor and the rate of the charge transfer process can be derived from the general classical Marcus theory [46]:

$$K_{inject} = \frac{|V_{RP}| (2/h (\pi/\lambda K_B T))^{1/2} \exp[-G_{inject} + \lambda] 2/4 K_B T}{\quad} \quad (13)$$

In Eq. (13), K_{inject} is the rate constant (in s^{-1}) of the electron injection from dye to TiO_2 , K_B is the Boltzmann thermal energy, h is the Planck constant, G_{inject} is the free energy of injection and V_{RP} is the coupling constant between the reagent and the product potential curves. Eq. (14) revealed that larger V_{RP} leads to higher rate constant which would result in a better sensitizer. The use of the generalized Mulliken-Hush (GMH) formalism allows evaluating V_{RP} for a photo-induced charge transfer [47]. It was explained that V_{RP} can be evaluated as follows [48]:

$$|V_{RP}| = \frac{\Delta E_{RP}}{2}. \quad (14)$$

The injection driving force can be formally expressed within Koopman's approximation as follows:

$$\Delta E_{RP} = [E_{LUMO}^{dye} + 2E_{HOMO}^{dye}] - [E_{LUMO}^{dye} + E_{HOMO}^{dye} + E_{CBO}^{TiO_2}] \quad (15)$$

where $E_{CBO}^{TiO_2}$ is the conduction band edge. It is difficult to accurately determine $E_{CBO}^{TiO_2}$, because it is highly sensitive to the operating conditions (e.g. the pH of the solution). Thus, we have used $E_{CBO}^{TiO_2} = -4.0\text{eV}$ [46] which is an experimental value corresponding to conditions where the semiconductor is in contact with aqueous redox electrolytes of fixed pH 7.0 [49-50]. More quantitatively, for a closed-shell system, E_{LUMO}^{dye} corresponds to the reduction potential of the dye E_{RED}^{dye} , whereas the HOMO energy is related to the potential of the first oxidation (that is, $E_{HOMO}^{dye} = E_{OX}^{dye}$). As a result, Eq. (15) becomes:

$$\Delta E_{RP} = E_{OX}^{dye} + E_{OX}^{TiO_2}. \quad (16)$$

According to Koopman's theory, the ground-state oxidation potential energy is related to ionization energy [51].

The photovoltaic properties λ_{max} , ΔG_{inject} , E_{OX}^{dye*} , E_{OX}^{dye} , λ_{max}^{CT} and LHE are presented in Table 11. The short-circuit current (J_{SC}) depends on two main influencing factors: light-harvesting efficiency (LHE) and the electronic injection free energy (ΔG_{inject}) (Eq. (10)). The LHE is considered as a very important factor for the organic dyes in which we could appreciate the role of the dyes in the DSSC; i.e., absorbing photons and injecting photo-excited electrons to the conduction band of the semiconductor

(TiO_2). In order to know what to give as an intuitional impression of the influence of the donor spacer of the LHE, we compared this research project with Juma *et al.* [20] and observed that the oscillator strengths were changing at different excitations. As shown in Table 11, the LHE has a value that's less than 1 and ΔG_{inject} is negative; these values reveal that the electron injection process is spontaneous [52] and m-diacetylaminoozopyrimidine at the excited state would be located above the conduction band edge of TiO_2 , resulting in a favorable condition for electron injection.

Also, comparing this research project with Juma *et al.* [20], it was observed that m-diacetylaminoozopyrimidine has a smaller ΔG_{inject} . Based just on LHE and ΔG_{inject} related to J_{SC} according to Bourass *et al.* [19], we could conclude that the dye-synthesized solar cell containing the m-diacetylaminoozopyrimidine should have the lowest J_{SC} due to its relatively small LHE and injection driving force.

From the calculation, it is revealed that m-diacetylaminoozopyrimidine has the smallest electron injection value due to its carbonyl (acetyl) as withdrawing group. With regard to light-harvesting efficiency which is responsible for power conversion efficiency, the higher the LHE, the higher the power conversion efficiency.

TABLE 11. Photovoltaic properties of dyes in gas phase.

Photovoltaic properties	Values obtained (eV)
E_{OX}^{dye}	-2.697
E_{OX}^{dye*}	-5.5
ΔG_{inject}	-8.59
(LHE)	0.060868
V_{OC}	1.303
$ V_{RP} $	-1.1515

4. Conclusion

This study being the maiden quantum mechanical/theoretical investigation on the hypothetical m-diacetylaminoozopyrimidine, complete vibrational and molecular structure analysis has been carried out using DMol3 Density Functional Theory (DFT) methods.

At the ground-state study, we observed that the molecular structure and geometry of m-diacetylaminoozopyrimidine were maintained

because of the resistance to alteration in electron distribution by chemical hardness. The highest occupied molecular orbital (HOMO) and the lowest unoccupied molecular orbital (LUMO) energies can be used to semi-quantitatively estimate the ionization potential, electron affinity, electronegativity, electrophilicity index, chemical potential, chemical hardness and chemical softness.

In order to understand electronic transitions and vibrations of m-diacetylaminoazopyrimidine at the excited state, TD-DFT calculations on FT-IR spectra in gas phase were also performed. It was observed that m-diacetylaminoazopyrimidine showed a distortion on the aromatic heterocyclic ring. Fukui function helps identify the electrophilic and nucleophilic nature of a specific site within the molecule. According to stability of the molecule to

softness, the molecule at least energy gap as compared with ground state and other research work is much more reactive.

It was observed that the high conjugated double bonds have both high absorption spectra and increased electron injection efficiency and the conjugations made the energy gap decrease at the excited state. Therefore, the investigation shows that m-diacetylaminoazopyrimidine is better for application in dye-synthesized solar cells (DSSCs).

Funding

Although this work was not supported by any funding agencies, the authors are thankful to Prof. Dr. Ayuk for his immense support and contributions.

References

- [1] Koh, J., Greaves, A.J. and Kim, J.P., *Dyes and Pigments*, 56 (1) (2003) 69.
- [2] Sekar, N., *Colourage*, 51 (2004) 59.
- [3] Katz, H.E., Lovinger, A.J., Johnson, J., Kloc, C., Siegrist, T., Li, W. and Dodabalapur, A., *Nature*, 404 (6777) (2000) 478.
- [4] Abe, H., Yoneda, M. and Fujiwara, N., *Japanese Journal of Applied Physics*, 47 (3R) (2008) 1435.
- [5] Chino, T. and Yamada, M., *J.P.*, (2002) 2001220519.
- [6] Wang, S., Shen, S. and Xu, H., *Dyes and Pigments*, 44 (3) (2000) 195.
- [7] Kuwahara, M., Takehara, S., Kashihara, Y., Watabe, K., Nakano, T., Tanaka, M., Nakamura, N., Ohsawa, H. and Satoh, H., *Jpn. J. Appl. Phys.*, 42 (2003) 1068.
- [8] Rangnekar, D.W., Kanetkar, V.R., Malanker, J.V. and Shankarling, G.S., *Indian Journal of Fibre & Textile Research (IJFTR)*, 24 (2) (1999) 142.
- [9] Hallas, G. and Choi, J.H., *Dyes and Pigments*, 40 (2-3) (1999) 119.
- [10] Gregory, P., Waring, D.R. and Hallos, G., "The chemistry and application of dyes". (Plenum Press, London, 1990), 18-20.
- [11] Kondil, S.S., *Transition Met. Chem.*, 23 (1998) 461.
- [12] Daniel, J.W., *Toxicology and Applied Pharmacology*, 4 (5) (1962) 572.
- [13] Woissetschläger, O.E., Sünkel, K., Weigand, W. and Beck, W., *Journal of Organometallic Chemistry*, 584 (1) (1999) 122.
- [14] Broekaert, J.A.C., Leis, F. and Laqua, K., *Talanta*, 28 (10) (1981) 745.
- [15] Amin, A.S. and Mohammed, T.Y., *Talanta*, 54 (4) (2001) 611.
- [16] Yazdanbakhsh, M.R., Yousefi, H., Mamaghani, M., Moradi, E.O., Rassa, M., Pouramir, H. and Bagheri, M., *Journal of Molecular Liquids*, 169 (2012) 21.
- [17] Gonçalves, L.M., de Zea Bermudez, V., Ribeiro, H.A. and Mendes, A.M., *Energy & Environmental Science*, 1 (6) (2008) 655.
- [18] Zhang, J., Li, H.B., Sun, S.L., Geng, Y., Wu, Y. and Su, Z.M., *Journal of Materials Chemistry*, 22 (2) (2012) 568.
- [19] Bourass, M., Benjelloun, A.T., Benzakour, M., Mcharfi, M., Hamidi, M., Bouzzine, S.M. and Bouachrine, M., *Journal of Materials and Environmental Science*, 7 (2016) 700.
- [20] Juma, J.M., Vuai, S.A.H. and Babu, N.S., *International Journal of Photoenergy*, 2019 (2019) 4616198.

- [21] Janjua, M.R.S.A., *Journal of the Chilean Chemical Society*, 63 (1) (2018) 3850.
- [22] Fleming, I., "Molecular Orbitals and Organic Chemical Reactions", (John Wiley & Sons, 2011).
- [23] Parr, R.G. and Yang, W., *Journal of the American Chemical Society*, 106 (14) (1984) 4049.
- [24] Parr, R.G., *International Journal of Quantum Chemistry*, 37 (4) (1990) 327.
- [25] Ali, M., Mansha, A., Asim, S., Zahid, M., Usman, M. and Ali, N., *Journal of Spectroscopy*, 2018 (2018) 9365153.
- [26] Yossa Kamsi, R.A., Ejuh, G.W., Tchoffo, F., Mkounga, P. and Ndjaka, J.M.B., *Advances in Condensed Matter Physics*, 2019 (2019) 4246810.
- [27] Demircioğlu, Z., Kaştaş, Ç.A. and Büyükgüngör, O., *Journal of Molecular Structure*, 1091 (2015) 183.
- [28] Mulliken, R.S., *J. Chem. Phys.*, 23 (1955) 1841.
- [29] Nazari, F. and Zali, F.R., *Journal of Molecular Structure: Theochem.*, 817 (1-3) (2007) 11.
- [30] Lee, C., Yang, W. and Parr, R.G., *Journal of Molecular Structure: Theochem.*, 163 (1988) 305.
- [31] Chattaraj, P.K., Maiti, B. and Sarkar, U., *The Journal of Physical Chemistry A*, 107 (25) (2003) 4973.
- [32] Muller, R.P. and Warshel, A., *The Journal of Physical Chemistry*, 99 (49) (1995) 17516.
- [33] Scott, A.P. and Radom, L., *J. Chem. Phys.*, 100 (1996) 16502.
- [34] Pulay, P., Fogarasi, G., Pongor, G., Boggs, J.E. and Vargha, A., *Journal of the American Chemical Society*, 105 (24) (1983) 7037.
- [35] Varsányi, G., "Assignments for vibrational spectra of seven hundred benzene derivatives", Vol. 1, (Halsted Press, 1974).
- [36] Temel, E., Alaşalvar, C., Eserci, H. and Açar, E., *Journal of Molecular Structure*, 1128 (2017) 5.
- [37] Pecsok, R.L., "Modern Methods of Chemical Analysis", (Wiley, 1976).
- [38] Sharma, Y.R., "Elementary Organic Spectroscopy: Principles and Chemical Application". (Chand and Company, Ltd., New Delhi, India, 2009).
- [39] Kalsi, P.S., "Spectroscopy of Organic Compounds", (New Age International, 2007).
- [40] Hohenberg, P. and Kohn, W., "Inhomogeneous Electron Gas *Physical Review* 136", (B864, 1964).
- [41] Marinado, T., Nonomura, K., Nissfolk, J., Karlsson, M.K., Hagberg, D.P., Sun, L.,... & Hagfeldt, A., *Langmuir*, 26 (4) (2010) 2592.
- [42] Zhang, J., Li, H.B., Sun, S.L., Geng, Y., Wu, Y. and Su, Z.M., *Journal of Materials Chemistry*, 22 (2) (2012) 568.
- [43] Ninis, O., Bouzzine, S.M., Toufik, H., Lamchouri, F., Abarkan, M., Hamidi, M. and Bouachrine, M., *Journal of Applied Chemical Research*, 7 (1) (2013) 19.
- [44] Barbara, P.F., Meyer, T.J. and Ratner, M.A., *The Journal of Physical Chemistry*, 100 (31) (1996) 13148.
- [45] De Angelis, F., Fantacci, S. and Selloni, A., *Nanotechnology*, 19 (42) (2008) 424002.
- [46] Marcus, R.A., *Angewandte Chemie, International Edition in English*, 32 (8) (1993) 1111.
- [47] Pourtois, G., Beljonne, D., Cornil, J., Ratner, M.A. and Brédas, J.L., *Journal of the American Chemical Society*, 124 (16) (2002) 4436.
- [48] Hsu, C.P., *Accounts of Chemical Research*, 42 (4) (2009) 509.
- [49] Asbury, J.B., Wang, Y.Q., Hao, E., Ghosh, H.N. and Lian, T., *Research on Chemical Intermediates*, 27 (4-5) (2001) 393.
- [50] Katoh, R., Furube, A., Yoshihara, T., Hara, K., Fujihashi, G., Takano, S. and Tachiya, M., *The Journal of Physical Chemistry B*, 108 (15) (2004) 4818.
- [51] Babu, N.S. and Jayaprakash, D., *HOMO*, 1 (2015) 1.
- [52] El Assyry, A., Jdaa, R., Benali, B., Addou, M. and Zarrouk, A., *Journal of Materials and Environmental Science*, 6 (9) (2015) 2612.